Ore Geology Reviews 115 (2019) 103034

Contents lists available at ScienceDirect

Ore Geology Reviews

journal homepage: www.elsevier.com/locate/oregeorev

Uranium occurrence state in the Tarangaole area of the Ordos Basin, China: Implications for enrichment and mineralization

Lulu Chen[a,b,*], Yin Chen[a], Xiaoxi Feng[a], Jian-guo Li[a], Hu Guo[a,b], Peisen Miao[a], Ruoshi Jin[a], Chao Tang[a], Hualei Zhao[a], Gui Wang[c], Shuguang Li[c]

[a] Tianjin Center, China Geological Survey, Tianjin 300170, China
[b] Laboratory of Non-Fossil Energy Minerals, Tianjin Center of China Geological Survey, Tianjin 300170, China
[c] CNNC Geological Party No. 208, Baotou, Inner Mongolia 014010, China

ARTICLE INFO

Keywords:
Ordos Basin
Sandstone-host uranium deposit
Uranium occurrence state
Tarangaole area
Uranium mineralization

ABSTRACT

The Zhiluo Formation in the Tarangaole area is a part of the Dongsheng uranium ore-field in the northeast Ordos Basin, China. Uraniferous sandstones from this formation are examined in this study. The type and mode of occurrence of uranium minerals is investigated in detail using an electron probe, α-track etching, energy spectrum, backscattering, a scanning electron microscope, and an experiment for sequential extraction of uranium. The results show that these uranium minerals are mainly composed of coffinite, a small amount of pitchblende, and some minerals containing titanium and uranium. Coffinite closely coexists with pyrite, altered ilmenite or leucoxene, charcoal, biotite and clay minerals. Some coffinite occurs along mineral edges as burrs or fine columns; it also occurs in biotite cleavage cracks with granulars. In addition, some uranium minerals are also observed within grains. α-Track etching shows that adsorbed uranium is either distributed at the edge of the debris or scattered among the grains. The sequential extraction experiment indicates that the proportion of uranium minerals was significantly greater than that of the adsorbed uranium in the samples, with the latter being largely present in pyrite and organic matter. Residual, oxidizable and weak acid-extractable uranium occur in the deposit. Scan-mapping of uranium and titanium reveals that brannerite is almost nonexistent. Strongly altered ilmenite is considered a highly effective aggregating agent for uranium. A large number of altered minerals, including clays, carbonaceous clastics, biotite, pyrite and ilmenite, are widely developed in the uraniferous sandstone, and play a significant role in the complex process of adsorption–reduction–precipitation of uranium. The discovery of pitchblende and two types of coffinite (high-Y and low-Y) are discussed in context with their symbiotic relationship with the altered minerals. It is suggested that the uraniferous sandstone underwent at least two stages of fluid activity.

1. Introduction

Uranium resource exploration in China focuses extensively on sandstone-type uranium deposits, in part due to their industrial value, but also because of their shallow depth, large-scale reserves, low-cost of mining, and environmental friendliness (Granger and Warren, 1974; Chen et al., 2003). Although research on sandstone-type uranium deposits has been carried out in considerable detail, not much has been done on uranium occurrence state – which involves understanding not only the metallogenic mechanism and enrichment regularity, but also the technological process and economic benefit of uranium mining. Many sandstone-type uranium deposits have been reported from the northeast Ordos Basin in recent years, including the Zaohuohao, Daying and Nalinggou uranium deposits (Yang et al., 2009; Miao et al., 2009, 2010; Ma et al., 2013; Wu et al., 2016; Wang et al., 2017; Akhtar et al., 2017). The Tarangaole area, which is the focus of this study, is located to the west of the Zaohuohao Deposit and east of the Daying Deposit (Fig. 1). The western part of this area is bordered by the Nalinggou deposit, which has been the subject of recent exploratory surveys by the Tianjin Center of the China Geological Survey. Together, the Tarangole and Nalinggou deposits constitute a large national uranium resource base.

Uranium occurrence has been studied using a variety of methods, including scanning electron microscopy and electron probe microanalysis (Doveton et al., 2004; Yang et al., 2006a; Reyes-Cortés et al., 2010; Decree et al., 2011; Zhao et al., 2014; Galindoet et al., 2007). Gallegos et al. (2015) conducted SEM testing and α-track analysis on uraniferous samples from the Wyoming sandstone-type uranium deposit. In low-grade ore, they found that uranium occurred on the

* Corresponding author at: Tianjin Center, China Geological Survey, Tianjin 300170, China.
E-mail address: luluchen1987@yeah.net (L. Chen).

https://doi.org/10.1016/j.oregeorev.2019.103034
Received 3 May 2018; Received in revised form 13 July 2019; Accepted 24 July 2019
Available online 25 July 2019
0169-1368/

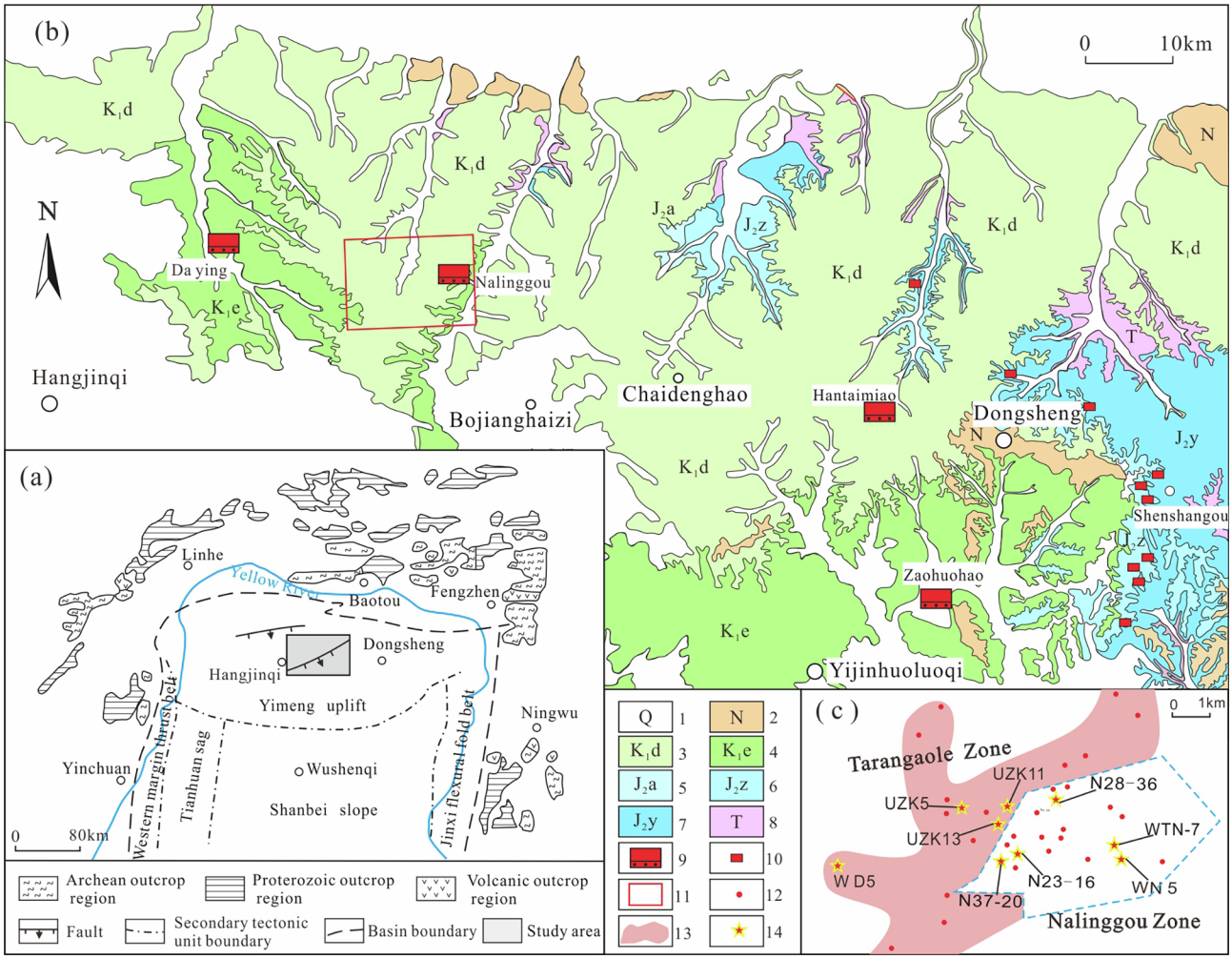

Fig. 1. Tectonic map of the study area. Abbreviations – numbered in the figure legend – are: (1) Quaternary; (2) Neogene; (3) Dongsheng Formation; (4) Ejin Horo Formation; (5) Anding Formation; (6) Zhiluo Formation; (7) Yan'an Formation; (8) Triassic; (9) uranium deposit; (10) uranium mineralization spot; (11) area of study; (12) mineralized borehole; (13) mineralized area in the Tarangaole area; (14) sampling locations.

periphery of clay/silicate minerals and organic matter, while in high-grade ore, uranium minerals were mainly hosted on the surface of altered chlorite or idiomorphic pyrite (other than strawberry-like pyrite) (Gallegos et al., 2015). Using EDS, high resolution mapping and SEM, Akhtar et al. (2017) examined the relationship between uranium minerals and secondary pyrite in the Dongsheng Deposit of the Ordos Basin; their results suggest that the activity of micro-organisms aid the ore-forming process. Related studies have also been conducted by Chinese researchers. Zhang et al. (2015) analyzed uranium ore samples from the Mengqiguer Deposit in the Yili Basin using α-track etching and EPMA. Their results show that occurrence of uranium minerals is usually accompanied by carbonization and pyritization, although uranium also occurred on the edge of quartz or feldspars, especially in the corrosion pits of quartz grains (Zhang et al., 2015).

Based on previous studies on uranium deposits in the northeast Ordos Basin, uranium minerals reported from this area are predominantly coffinite, ursilite and a small amount of pitchblende, apart from adsorbed uranium (Wu et al., 2016; Wang et al., 2017); coffinite occurs in the fissures of altered biotite or at the edge of pyrite (Yang et al., 2009; Miao et al., 2009, 2010). Uranium in the Hangjinqi Deposit exists mostly in the mineral form; it is also adsorbed on the surface of pyrite or carbonate minerals (Ma et al., 2013); small amounts of uranothorite and brannerite, identified by EPMA analysis, also occur in this deposit (Ma et al., 2013; Song, 2013). In the Tarangaole area, pitchblende is found to be closely associated with coffinite. It is curious that pitchblende is seldom found in this area, as compared to other deposits in the Mesozoic-Cenozoic basins in northern China. Similarly, evidence for the local occurrence of brannerite, a medium-high temperature uranium mineral, is absent. If it is nonexistent, how can titanium and uranium be distributed in this mineral? The proportion of adsorbable uranium and the occurrence relationship between uranium and paragenetic minerals also need to be further ascertained. Based on α-track etching, EPMA, backscattering images, energy spectrometry, scanning electron microscopy and chemical sequential extraction, this paper systematically investigates uranium minerals, their occurrence forms and percentage in the area – with emphasis on the co-occurrence relationship between uranium and altered minerals. It is expected to complement and improve current understanding of the uranium occurrence state and metallogenic regularity in the Tarangaole area, and indeed the whole northeastern part of the Ordos Basin.

2. Geologic setting

The Ordos Basin lies in the western part of the North China. The north of the basin is adjacent to the Yinshan–Langshan mountains. It lies in a transition zone between two different dynamic settings: the marginal Pacific region and the Tethyan–Himalayan area, and is a superposed basin with an unstable inner craton (Yang, 2002; Xue et al., 2010). The Tarangaole area, in the northeast Ordos Basin, occurs on the southern margin of the Yimeng Uplift (Fig. 1a). It is bounded by the

Hetao Graben to the north and the Shanbei Slope to the south. Intense denudation in the north had led to the outcropping of Triassic, Jurassic, Cretaceous, Neogene and Quaternary deposits; of these, the Lower Cretaceous rocks are exposed the most (Fig. 1b).

The main uranium ore-bearing stratum in the study area is a member of the Lower Zhiluo Formation, the bottom of which directly overlies the bleached sandstone of the Yan'an Formation, across an anglular unconformity. The sedimentary environment under which the ore-bearing layer was deposited is recognized as a braided stream. The 100–200 m thick stratum occur as monoclines with mild dip angles of 1–3°. The rock color in the upper part is green to grayish green, while the lower part is gray, and the lithology is mainly medium- to coarse-grained sandstone with loose sand and low consolidation. Gray sandstone is relatively rich in reducing components, such as carbonaceous clastics and pyrite. In particular, the ore-bearing sandstone displays signs of weak carbonization. The sand body contains several positive cycles from bottom to top; boulder and boulder-clay are frequently seen at the bottom of the cycle (Fig. 2). It shows a distinct sedimentary characteristic of multi-stage superposed channels. Trough and tabular cross-beddings are also observed in the cycle. Uranium mineralization is controlled by the boundary between the green and gray sandstones (Wu et al., 2016); uranium tends to occur in the gray sandstone. Moreover, the ore body is tabular or lentiform in this area (Fig. 2).

3. Samples and analytical methods

Our study is focused on the rich ore in the Tarangaole area. Twenty-one probe sections of uraniferous sandstone samples were collected from nine industrial uranium ore drill holes (Fig. 1c). The distribution of adsorbed uranium and uranium minerals was analyzed by *α*-track etching, after which the altered mineral assemblage was observed under the electron microscope, and point concentrated areas were marked with circles. The different types of uranium minerals and their symbiotic relationship were analyzed using EPMA, energy spectrometry, scanning electron microscopy and backscattering analysis. The proportions of different uranium occurrence forms were tested by a quantitative analysis method of chemical sequential extraction, which allows speculation about metallogenesis and the enrichment mechanism of sandstone-type uranium deposits.

α-track etching and microscopy were performed at the Laboratory of Non-fossil Energy Minerals at the Tianjin Center of the China Geological Survey. The films were placed in 100 ml NaOH solution (10%), and rinsed, after which they were cut and fixed over the probe section with a wide clamp, and then numbered. These films were placed in a dark environment for 30 days, allowing radiation to accumulate, after which they were etched in a strong alkaline solution (40 g KOH + 5 g $KMnO_4$ + 100 ml H_2O) for 60 min at 60–65℃. These films were soaked in 1:1 HCl, and then rinsed and air dried for observation under an electron microscope, where they were photographed.

EPMA analysis was conducted at the Analytical Laboratory, CNNC Beijing Research Institute of Uranium Geology and the Laboratory of Non-Fossil Energy Minerals at the Tianjin Center of the China Geological Survey, using HEOL's JXA-8100 electron microprobe at acceleration voltage of 20 kV, with beam current = 1×10^{-8}A and beam spot diameter of 1 μm. The exit angle was 40°. Wave spectrum analysis was also performed.

Scanning electron microscopy was carried out at the Laboratory of Non-Fossil Energy Minerals at the Tianjin Center of the China Geological Survey, using a SS550 scanning electron microscope at an acceleration voltage of 15 kV, with beam spot diameter 10 nm and at a working distance of 5–10 mm.

The chemical sequential extraction experiment was conducted at the Analytical Laboratory, CNNC Beijing Research Institute of Uranium Geology, using an HR–ICPMS test method. The five states of uranium extracted were water-soluble, weak-acid extracted, reducible, oxidable, and residual state. They were leached and tested in the experiment by a series of procedures, such as dissolution, filtration, oxidization, heating, ignition, and so on.

4. Results

4.1. α-Track etching

α-Track etching is a method of examining the distribution and existence of different forms of uranium in ores (Qin et al., 2009; Xu et al., 2010). It is very effective in looking for fine-grained uranium and uraniferous minerals in thin sections. The distribution of α-tracks in dense veinlets, clumps or in radial forms is caused by X-rays from the radioactivity attenuation of a uranium mineral, while distribution in the form of sparse stars possibly signifies the dispersed adsorbed uranium or isomorphic uranium (Wang et al., 1989; Cun et al., 2016).

The distribution and scale of tracks were observed under the electron microscope, and the uranium relationship with symbiotic minerals was analyzed in the same view. Large amounts of adsorbed uranium with sporadic scattered points as well as numerous uranium minerals in the form of dense points were discovered in the films (Fig. 3A, a, B, b, C and c). By comparing the same view of plane polarized light of a probe section and etched film in the same sight, it was revealed that tracks mainly existed in fissures or coexisted with carbonaceous clastics, ilmenite and pyrite. Some tracks were distributed at the edge of grains (such as quartz or feldspar) or in the clay minerals in the form of dispersed points. Only a few tracks existed in zircon or rutile isomorphs.

4.2. Types of uranium minerals and their occurrence states

The analysis of EPMA, energy spectrometry and backscattering images indicated that the uranium minerals in the Tarangaole area were mainly coffinite, with a small amount of uraniferous–titaniferous mineral, pitchblende and uranothorite. Generally, uranium minerals contain a certain amount of water and hydroxyl (Min et al., 1992; Zhang et al., 1995). Since the electron probe could not detect the content of hydroxyl, carboxy and organic matter, the total composition is less than 100%, but it does not affect the qualitative discrimination of uranium mineral species.

1) As a result of the presence of a certain amount of H_2O in coffinite, the total chemical composition accounts for 81.14–98.46%, as reported in Table 1. This composition includes approximately 55.27–77.23% UO_2, 12.08–21.61% SiO_2, and about 1.9–4.3% CaO, 0–7.3% Y_2O_3, and 0–3.4% TiO_2, together with a small amount of FeO, Al_2O_3, MgO, Na_2O, SO_3 and K_2O. The average content of UO_2 was 64.64%, and SiO_2 on an average was 18.86%. Coffinite was mainly found in intergranular pores, coexisting with altered limonite, anatase, leucosphenite (TiO_2), pyrite, carbonaceous clastics or clay membranes (Fig. 4). Most of coffinite occurred in irregular forms at the periphery of clay minerals, altered ilmenite and pyrite (Fig. 4A, B and E). However, part of coffinite occurred as burrs or in micro-columnar form, and is closely associated with anatase or leucosphenite. Some coffinite originated in the cleavage cracks of biotite (Fig. 4C), and some veins of coffinite filled fissures in pyrite (Fig. 4F). A circle of coffinite grew along the rim of granular pyrite, followed by a thin layer of pyrite in some circumstances; both these layers were eventually cemented by calcite, that was deposited last.
2) Pitchblende, a type of uranium mineral rarely seen in this area, was identified in our analysis. It contained approximately 85.35–87.47% UO_2, and as little as 3.91–4.74% SiO_2. It also contained approximately 4% CaO; no Y element was tested for this mineral. Backscattering images indicated that the pitchblende coexisted with coffinite, usually wrapped around the coffinite core (Fig. 4D). The color of pitchblende in the backscattering image was brighter than coffinite, and the boundary was irregularly serrated. A preliminary conclusion was that it was the altered residue of primary uranium minerals.
3) Individual EPMA and EDS data indicated the presence of Ti and U in the uranium mineral component. Point composition data suggests that it contained 8.29–13.73% SiO_2, 33.97–56.35% UO_2,

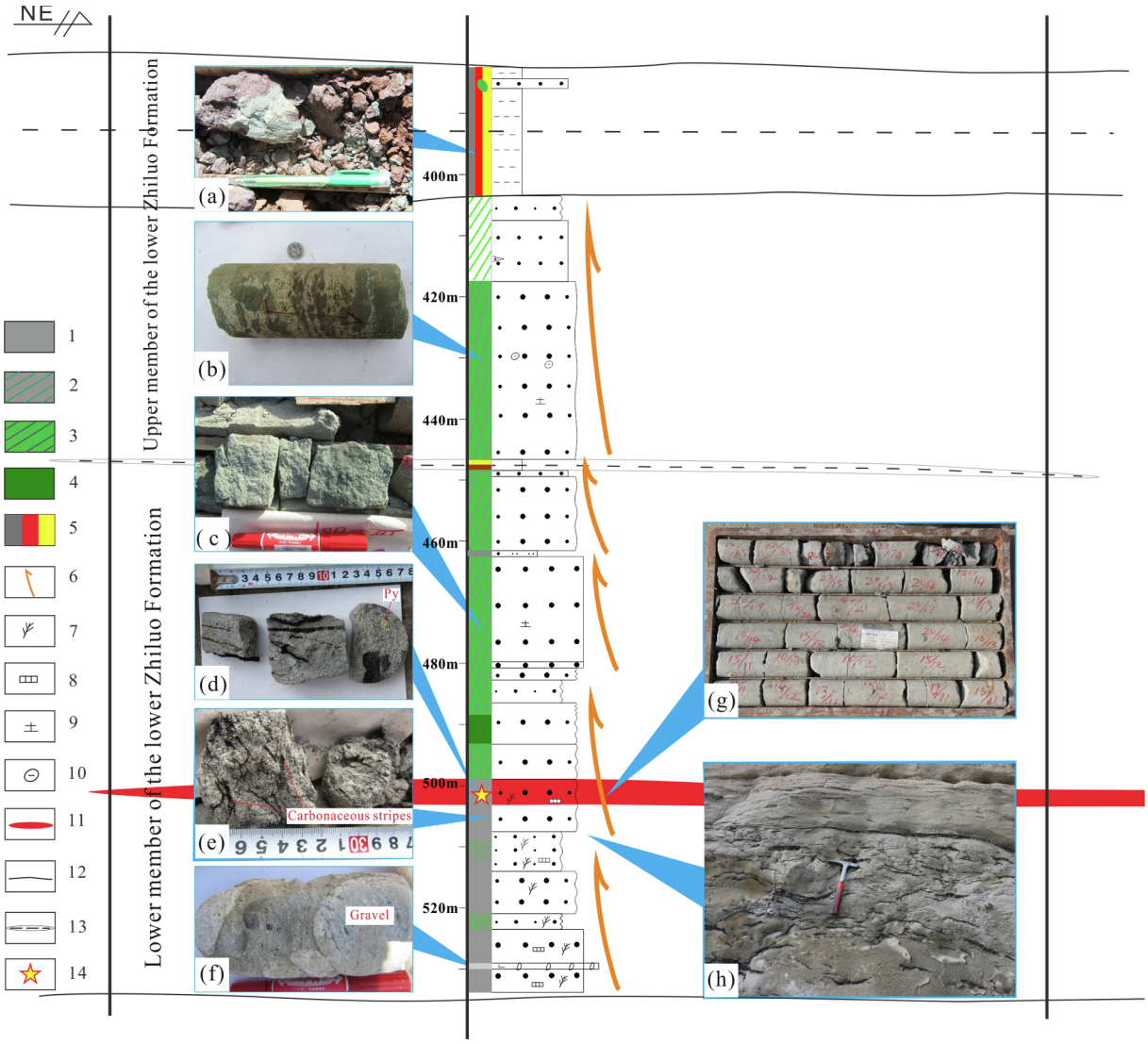

Fig. 2. Characteristics of ore-bearing strata and field photographs from the Tarangaole area. (a) The variegated mudstone is brownish-red with green spots. (b) Several green and reddish-brown irregular boulders in the grayish-green medium-coarse sandstone at 430 m depth. (c) Grayish-green loose coarse sandstone at 474 m depth. (d) Organic detritus, pyrite and weak carbonation seen in the gray medium-to-coarse uraniferous sandstone at 501 m depth. (e) Several carbonaceous stripes in the light gray loose sandstone at 506 m depth. (f) Light gray calcium-cemented glutenite with gravel, that is rounded and varies in size, at 530 m depth. (g) Gray ore-bearing sandstone in the core, from 409 to 504 m depth. (h) Bedding and numerous carbonaceous bands are visible in the lower section of the Zhiluo Formation in the outcrop profile of the Shenshan valley. Colors and notations – numbered in the figure legend – are: (1) gray, (2) green-gray, (3) greyish-green, (4) green, (5) motley, (6) sedimentary cycle, (7) organic detritus, (8) pyrite, (9) kaolinization, (10) boulder clay or gravel, (11) uranium ore body, (12) stratigraphic boundary, (13) argillaceous interlayer, and (14) sampling locations. (For interpretation of the references to color in this figure legend, the reader is referred to the web version of this article.)

0.98–1.63% CaO, 2.11–12.66% FeO, and 17.61–36.24% TiO_2; the percentage composition of TiO_2 and UO_2 vary (Table 1), and the content of UO_2 can be positively correlated with SiO_2. Previous studies showed a wider range of content for both TiO_2 and UO_2. In Table 1, the mineral "brannerite" contains 4.47–18.07% SiO_2, 8.09–55.5% UO_2, 0.83–2.14% CaO, 1.54–4.64% FeO, and 6.78–59.40% TiO_2. The percentage composition of TiO_2 and UO_2 was not consistent with that of brannerite (Zhang et al., 1995), so it was called a uraniferous–titaniferous mineral in the text. The occurrence state of this kind of uranium mineral was similar to coffinite. It was usually associated with altered ilmenite and leucosphenite. Most of the minerals were distributed in the margins or fractures of the mineral.

4) Only one unconfirmed uranothorite was discovered in this study. The mineral contained 21.08% SiO_2, 24.61% UO_2, 2.59% CaO, 1.18% Al_2O_3, 1.28% Y_2O_3, 0.2% TiO_2, 0.85% ZrO_2 and 39.67% ThO_2. EPMA analysis and backscattering images indicated that the primary mineral may be sphene (Fig. 4G). The lower part was intact, while the upper was fractured. The fractured part was uraniferous because uranium probably entered the mineral by adsorption or isomorphism.
5) Some uranium minerals were also found in feldspar, rock debris (Fig. 4H); these might be an indicator of their provenance.

4.3. Chemical sequential extraction experiment

The objective of chemical sequential extraction is to erode or exchange each form of an element in a sample by using different chemical reagents in sequence, from weak to strong. The purpose is to separate a geochemical phase from every step and detect the element content in each of the phases (Song, 2004; Ma et al., 2012, 2013; Zheng et al., 2015; Cun et al., 2016). In this study, five high-grade ore samples were selected. Five states of uranium (water-soluble, weak acid-extractable,

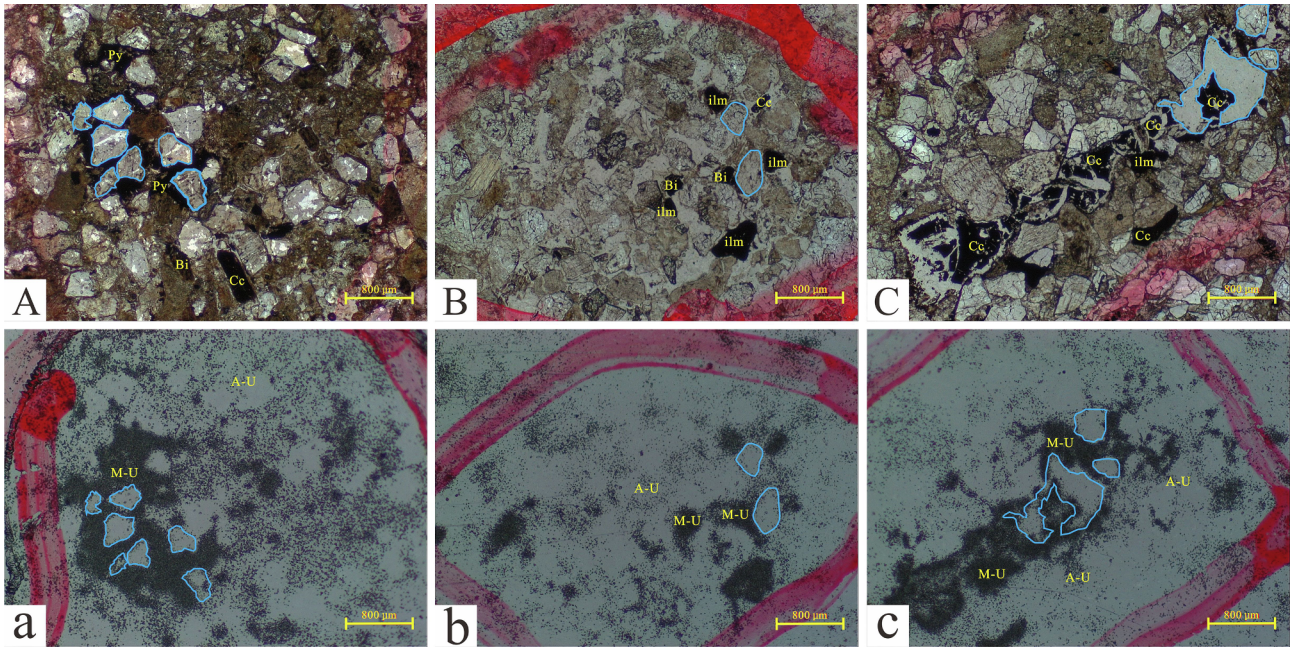

Fig. 3. The distribution of α-track from the thin sections of the ore-bearing rock. (A-a) Photographs from the probe section 15nzk006 and etched tracks of the same scene; α-tracks mainly appear on the edge of grains in the form of dense clumps. (B-b) Photographs of the probe section 15nzk006 and etched tracks of the same scene. (C-c) Photographs of the probe section 15nzk005 and etched tracks of the same scene; α-tracks coexist along with organic detritus in the form of dense clumps. Abbreviations: Cc, carbonaceous clastics; Py, pyrite; Bi, biotite; ilm, ilmenite; A–U, adsorption state of uranium; M – U, uranium mineral.

reducible, oxidable, and residual) were extracted by using the Tessier method. The results are presented in Table 2.

For the water-soluble state or exchangeable ionic state, diffuse ion adsorption and outer-sphere complexation allowed the added reagent to extract the metallic ions adsorbed on the sediment surface quickly. The results showed that the uranium element in the water-soluble state accounted for 0.45–4.6%, with an average of 1.92% (Table 2). The low proportion suggested that only a small amount of uranium was adsorbed on the surface of clay minerals through diffusion.

For the weak acid-extractable or carbonate-bonded state, elemental uranium occurring in carbonate minerals that form by precipitation or co-precipitation, such as calcite, dolomite or rhodochrosite, were extracted with acetic acid, which normally do not disrupt iron and manganese oxides in the sample. This acid also does not have any adverse effect on organic matter. The results showed that uranium in the carbonate-bonded state accounted for a high proportion of their occurrence at 13.75–35.41%, with an average of 26.98% (Table 2).

The reducible state or iron-manganese oxidized state indicates the portion produced by the heavy metal ion, when reacted with iron oxyhydroxide or manganese oxide in water. The most typical character of this phase was poor stability in the reducing environment; generally, it could be dissolved in a hydroxylamine hydrochloride solution. In the five samples analyzed, uranium in the reducible state took the lowest proportion at approximately 0.22–6.32%, with an average of 1.32% (Table 2).

In the oxidizable or organic-pyrite bonded state, uranium adsorbed on the surface of organic or pyrite grain in different forms, or chelated with organic matter is extracted. During the extraction, organic matter is completely oxidized. The most commonly used extraction agent is H_2O_2, which can dissolve manganese oxides in the sample and so, cannot be used until the third state was extracted. In these samples, uranium in the oxidizable form accounted for a fairly high proportion, at 7.71–32.44%, with an average of 14.45% (Table 2).

In the residual state, uranium generally occurs in primary or secondary silicates, or as stable uranium minerals and some uraniferous minerals. The uraniferous mineral usually forms as a result of adsorption or isomorphism. Uranium in this state was detected in all the samples, and it was also the most important part, accounting for the largest contribution at 31.91–77.68% of the total uranium, with an average of 55.43% (Table 2).

The average proportion of uranium in each of the five states is summarized as – residual state (55.43%) > weak acid-extractable state (26.98%) > oxidizable state (14.45%) > water-soluble state (1.92%) > reducible state (1.32%). According to previous findings (Wu et al., 2016), the residual state and weak acid-extractable state were the major forms of occurrence for the uranium element. The data from this experiment indicates that uranium in these two states accounts for 65.22–91.43%, with an average of 82.41%. The three adsorbed states of uranium (oxidizable, water-soluble, and reducible) account for 8.57–35.3%, with an average of 17.59% (Table 2). Data analysis showed that the uranium from the Tarangaole area mainly exists in mineral form and in the adsorbed form, and that the uranium concentration from minerals is higher than that of adsorbed uranium. In addition, the uranium in the organic-pyrite bonded state – in pyrite and organic matter – was dominant in the adsorbed form, while the other adsorbed forms, together, account for a much smaller share.

Based on data from a few samples collected from the Daying and Hangjinqi uranium deposits, previous authors suggested roughly equal proportions of uranium occurrence, in the mineral and adsorbed forms (Cun et al., 2016; Wu et al., 2016). It conflicts with our results from the experiment; this could possibly be due to the limited number of samples, and their highly divergent compositions. The results presented in Fig. 5 and Table 2 demonstrate a notably lower proportion of the pyrite-organic bonded form and a higher proportion of the residual form in our samples. Samples 16nzk027, 16nzk043 and 16nzk054 contained plenty of organic detritus, and the total amount of uranium and the percentage of its forms of occurrence showed considerable variations. The pyrite content could be a contributor, despite different levels of calcite cementation. In fact, a small amount of sporadic and macroscopic pyrite was observed in 16nzk054.

Furthermore, the comparison of test data reveals a notably higher proportion of weak acid-extractable uranium in the higher-grade samples at approximately 34–35%, as compared to the lower-grade samples, such as 16nzk033, 16nzk032, 16nzk054 and 2014DY-36 (Table 2). In the lower-grade samples, 16nzk027, 16nzk043, 2014DY-32 and

Table 1
Electron microprobe data for uranium minerals for mineralized sandstone samples in the Tarangaole area. Table 1. The data of electron probing analyses for uranium minerals from the samples of the mineralized sandstone in Tarangaole area.

SN	Test Point	Test Result (%)																Type of Uranium Mineral
		Na_2O	SiO_2	UO_2	FeO	Al_2O_3	MgO	CaO	TiO_2	Y_2O_3	SO_3	MnO	K_2O	PbO	ZrO_2	ThO_2	P_2O_5	Total	
1	15nZK004-2	0.08	17.23	55.27	0.37	0.98	0.24	1.36	2.37	5.63	0.12	/	0.18	/	/	/	1.03	84.86	Coffinite
2	15nZK004-3	0.28	19.08	59.39	0.18	1.19	0.12	0.81	0.23	6.26	0.65	/	0.25	/	/	/	1.23	89.67	Coffinite
3	15nZK004-4	0.32	18.33	57.92	0.34	0.92	0.12	1.42	0.17	6.06	0.22	/	0.15	0.12	/	/	1.17	87.26	Coffinite
4	15nZK004-5	0.34	19.12	58.21	0.08	0.96	0.15	1.52	0.82	5.97	0.12	/	0.20	0.10	/	/	1.19	88.78	Coffinite
5	15nZK004-6	0.38	16.71	55.68	1.62	0.90	0.20	0.96	0.27	5.78	1.20	/	0.16	/	/	/	1.12	84.98	Coffinite
6	15nZK004-8	0.43	17.61	52.49	0.68	0.98	0.23	1.13	0.24	5.62	0.26	/	0.32	/	/	/	1.15	81.14	Coffinite
7	15nZK004-9	0.56	19.81	58.46	0.65	1.47	0.93	2.19	0.16	6.36	0.11	/	0.24	/	/	/	1.23	92.17	Coffinite
8	15nZK004-10	0.39	20.49	56.99	0.58	1.57	0.14	2.10	/	6.53	0.08	/	0.20	/	/	0.08	1.19	90.34	Coffinite
9	15nZK004-12	1.04	18.78	58.19	0.20	1.07	0.11	2.08	1.25	5.94	0.19	/	0.18	/	0.08	/	1.21	90.32	Coffinite
10	15nZK004-13	0.36	19.33	62.54	0.43	1.04	0.21	1.93	1.74	5.60	0.31	/	0.17	/	/	/	1.23	94.89	Coffinite
11	15nZK004-15	0.18	19.83	59.76	2.46	1.20	0.11	0.50	0.30	3.87	2.29	/	0.28	/	/	/	0.71	91.49	Coffinite
12	15nZK004-18	0.14	19.38	62.58	0.33	1.31	0.16	0.99	0.17	1.77	0.06	/	0.25	/	/	/	0.50	87.64	Coffinite
13	15nZK007-1	0.43	19.25	64.83	0.23	1.56	0.21	2.62	1.56	1.28	0.04	0.05	0.24	/	0.37	0.26	0.43	93.36	Coffinite
14	15nZK007-2	0.39	19.57	70.58	0.23	1.37	/	2.09	/	0.62	/	/	0.20	0.10	/	/	0.31	95.46	Coffinite
15	15nZK007-3	0.21	20.45	63.55	0.24	1.70	0.05	2.03	2.39	1.37	/	/	0.17	/	0.23	/	0.56	92.95	Coffinite
16	15nZK007-4	0.67	20.44	62.50	0.27	1.79	0.16	2.50	1.00	1.00	0.02	/	0.19	/	0.23	/	0.45	91.22	Coffinite
17	15nZK007-5	0.93	20.35	66.92	0.49	1.51	0.11	1.92	0.32	1.05	0.10	/	0.21	/	/	/	0.44	94.35	Coffinite
18	15nZK007-6	0.60	20.78	64.48	0.10	1.63	0.06	2.14	0.20	1.15	/	/	0.21	/	/	/	0.56	91.91	Coffinite
19	15nZK007-7	0.61	20.22	62.57	0.20	1.65	0.11	2.26	2.41	1.11	0.04	/	0.16	/	0.38	0.08	0.48	92.28	Coffinite
20	15nZK007-8	0.34	20.77	67.59	0.15	1.35	0.02	1.99	0.94	1.14	/	/	0.22	/	/	/	0.57	95.08	Coffinite
21	15nZK019-2	0.50	4.74	85.04	0.93	0.38	/	4.14	0.80	/	/	0.08	0.25	0.20	0.09	/	0.08	97.23	Pitchblende?
22	15nZK019-3	/	19.67	69.49	0.07	1.25	/	2.55	1.56	/	/	/	0.25	/	/	/	0.63	95.47	Coffinite
23	15nZK019-4	0.56	3.91	87.47	0.87	0.38	0.03	4.00	/	/	/	0.08	0.23	0.09	/	/	0.22	97.84	Pitchblende?
24	15nZK019-5	0.98	4.09	85.35	1.09	0.28	0.02	4.77	0.46	/	/	0.05	0.29	/	/	/	0.13	97.51	Pitchblende?
25	15nZK019-6	0.61	15.34	73.05	0.19	0.95	/	3.21	0.72	0.15	0.02	/	0.31	/	0.09	/	0.50	95.14	Coffinite
26	15nZK019-7	0.34	20.02	70.48	0.44	1.39	0.04	2.41	0.13	0.32	0.04	/	0.20	/	0.07	/	0.78	96.66	Coffinite
27	15nZK019-8	0.46	19.59	72.97	0.61	1.37	0.03	2.28	0.41	0.20	/	/	0.22	/	/	/	0.32	98.46	Coffinite
28	15nZK019-9	0.67	19.44	70.64	1.02	1.59	0.39	2.31	0.26	0.07	/	/	0.25	/	/	/	0.30	96.94	Coffinite
29	15nZK019-10	0.43	20.73	69.98	0.37	1.55	0.08	2.26	0.25	0.23	0.03	/	0.25	/	/	/	0.49	96.65	Coffinite
30	15nZK019-11	0.39	14.89	75.64	0.51	1.12	/	2.31	0.58	/	0.02	0.11	0.28	0.16	/	/	0.23	96.24	Coffinite
31	15nZK019-12	0.16	21.61	66.79	1.00	1.48	0.06	2.16	0.12	0.25	0.27	/	0.21	0.50	/	/	0.53	95.14	Coffinite
32	15nZK019-13	0.61	17.84	69.56	0.15	1.22	0.06	2.09	0.16	0.61	0.05	/	0.22	/	0.06	0.07	0.34	93.04	Coffinite
33	15nZK019-14	0.25	19.8	69.61	0.15	1.30	/	2.36	0.63	0.97	0.02	0.04	0.21	/	/	/	0.56	95.90	Coffinite
34	15nZK019-15	0.25	15.14	71.75	0.20	1.14	/	2.43	0.47	0.36	0.14	/	0.26	/	0.13	/	0.39	92.66	Coffinite
35	15nZK019-16	0.24	20.23	68.89	0.05	1.39	0.06	3.16	0.22	0.44	0.04	/	0.23	0.14	0.11	/	0.92	96.12	Coffinite
36	15nZK019-17	0.62	18.82	66.29	0.23	1.64	0.04	2.17	0.42	0.75	/	/	0.41	/	/	/	0.46	91.85	Coffinite
37	15nZK019-18	0.28	15.67	71.17	0.24	1.22	0.02	2.68	0.65	0.52	0.03	/	0.22	0.18	/	/	0.51	93.39	Coffinite
38	15nZK019-19	0.68	17.52	70.28	0.11	1.27	/	2.47	0.13	0.83	/	/	0.27	/	/	/	0.54	94.10	Coffinite
39	15nZK019-20	0.24	19.67	65.32	0.22	1.41	0.03	4.33	0.39	1.43	0.11	/	0.21	/	0.06	/	1.07	94.49	Coffinite
40	15nZK019-21	0.23	15.14	68.17	0.20	1.21	0.04	2.98	2.43	0.64	/	/	0.21	/	0.05	/	0.64	91.94	Coffinite
41	15nZK019-22	0.39	12.08	77.23	0.29	0.93	/	2.48	0.20	0.23	/	/	0.22	/	0.05	/	0.39	94.49	Coffinite
42	15Wn5-K17-1	0.54	18.93	62.30	0.15	1.06	0.04	2.50	0.14	3.74	0.13	/	0.22	/	/	/	0.84	90.59	Coffinite
43	15Wn5-K17-2	0.74	17.96	57.47	0.69	1.69	0.18	2.67	/	3.89	0.18	/	0.25	/	/	/	0.65	86.37	Coffinite
44	15Wn5-K17-3	0.21	17.53	62.43	0.54	1.00	0.06	2.49	0.25	3.77	0.14	/	0.19	/	/	/	0.77	89.38	Coffinite
45	15Wn5-K17-4	0.83	19.25	62.27	0.36	1.08	0.09	3.14	0.20	3.30	0.09	/	0.20	/	/	0.09	0.97	91.87	Coffinite
46	15nZK042-1	0.54	20.33	56.80	0.54	1.11	0.04	1.49	0.22	7.30	0.51	/	0.21	0.14	/	/	0.90	90.13	Coffinite
47	15nZK048-1	0.26	21.08	24.61	0.12	1.18	/	2.59	0.20	1.28	/	/	0.10	/	0.85	39.67	0.85	92.79	Uranothorite
48	15nZK048-2	0.62	20.95	64.65	0.16	1.41	0.05	2.21	0.21	2.22	/	/	0.20	0.20	/	0.10	0.49	93.47	Coffinite
49	15nZK048-3	0.22	19.06	64.73	0.98	1.01	0.03	1.95	3.41	2.02	0.02	/	0.17	0.11	/	/	0.41	94.12	Coffinite
50	15nZK048-4	0.23	18.62	56.27	0.22	0.75	0.05	2.40	0.66	1.34	/	/	0.17	0.08	0.07	1.20	0.50	82.56	Coffinite
51	15nZK049-1	0.49	20.03	61.26	0.37	1.30	0.03	2.70	0.60	1.94	/	/	0.23	/	0.18	/	0.30	89.43	Coffinite
52	TU12-1	0.45	10.79	46.36	2.104	0.66	0.06	1.31	36.24	0.11	/	0.07	/	/	/	0.03	0.25	98.44	Uraniferous–titaniferous Mineral
53	TU12-2	0.69	12.01	50.69	5.06	0.78	0.07	1.53	19.74	0.14	/	0.2	/	/	/	0.03	0.27	91.21	Uraniferous–titaniferous Mineral
54	TU12-4	0.47	9.33	38.84	12.11	0.57	0.05	1.16	30.37	0.06	/	0.29	/	/	/	/	0.22	93.45	Uraniferous–titaniferous Mineral
55	TU12-5	0.35	10.87	47.24	6.72	0.61	0.02	1.31	28.22	0.06	/	0.18	/	/	/	/	0.22	95.80	Uraniferous–titaniferous Mineral
56	TU12-6	0.16	13.73	56.35	4.95	0.84	/	1.63	17.61	/	/	0.08	/	/	/	0.01	0.31	95.67	Uraniferous–titaniferous Mineral
57	TU12-7	0.45	8.29	33.97	12.66	0.53	0.05	0.98	34.44	0.03	/	0.14	/	/	/	0.04	0.17	91.75	Uraniferous–titaniferous Mineral
58	13-2	1.06	6.97	62.03	0.09	/	/	5.78	3.12	/	/	/	/	/	/	/	/	79.05	Ursilite
59	13-4	0.16	4.06	67.20	1.79	0.14	0.10	4.32	2.86	/	0.50	/	/	/	/	/	/	81.04	Ursilite
60	36-3-1-5	0.08	9.65	70.15	/	/	/	4.02	0.39	/	/	/	/	/	/	/	/	84.29	Ursilite
61	36-2-5-1	0.47	7.22	69.94	/	/	/	4.03	0.82	/	/	0.01	/	/	/	/	/	82.49	Ursilite
62	36-2-5-2	0.52	6.83	71.40	/	/	/	3.79	0.63	/	/	0.06	/	/	/	/	/	83.23	Ursilite
63	36-2-5-4	0.70	8.54	63.26	0.06	0.30	0.18	4.59	1.18	/	/	/	/	/	/	/	/	78.81	Ursilite
64	DY-8	0.33	17.6	62.14	0.21	1.34	0.01	1.24	0.12	5.28	0.08	0.14	/	/	/	/	/	88.50	Coffinite
65	DY-10	0.53	17.86	64.93	0.1	1.30	0.03	1.79	0.16	0.82	0.03	0.02	/	/	/	0.25	/	87.99	Coffinite

(*continued on next page*)

Table 1 (*continued*)

SN	Test Point	Test Result (%)																Type of Uranium Mineral
		Na_2O	SiO_2	UO_2	FeO	Al_2O_3	MgO	CaO	TiO_2	Y_2O_3	SO_3	MnO	K_2O	PbO	ZrO_2	ThO_2	P_2O_5	Total	
66	HJQ-035	0.22	13.85	38.8	1.54	0.30	/	0.83	32.53	0.48	/	0.20	/	0.10	/	/	/	89.02	Brannerite
67	DY-32	0.42	18.07	55.5	2.63	1.07	0.05	1.22	6.78	3.85	0.06	0.09	/	/	/	/	/	90.07	Brannerite
68	D31-1	0.09	4.47	11.41	4.25	1.23	0.19	2.14	59.23	/	/	/	/	/	/	/	/	83.01	Brannerite
69	D31-2	0.39	4.80	8.62	4.41	2.03	0.34	1.69	56.71	/	/	/	/	/	/	/	/	78.99	Brannerite
70	D31-3	0.41	5.89	8.09	4.64	2.16	0.44	1.68	59.40	/	/	/	/	/	/	/	/	82.71	Brannerite
71	DT-001	0.13	1.34	78.60	0.57	0.29	0.13	13.01	0.07	/	/	0.48	0.26	0.85	/	/	0.07	95.78	Pitchblende
72	DT-005	0.46	8.66	84.69	0.25	1.53	0.33	4.61	1.00	/	/	0.16	0.29	/	/	/	0.05	92.02	Pitchblende

Note: (1) Rows (serial numbers) 1–57, this study; 58–63, from Miao et al. (2010); 64–67, from Wu et al. (2016); 68–72, from Wang et al. (2017) . (2) Analysis for this study was done at the Analytical Laboratory, CNNC Beijing Research Institute of Uranium Geology using a JXA-8100 electron probe and energy spectrometer at an acceleration voltage = 15.0 kV, electron beam spot = 1 μm, and probe beam current = 2.00×10^{-8}A. Here, "/" indicates that the item is not detected or that its content is lower than the detection limit of the instrument.

2014DY-34, the data also shows a lower proportion of weak acid-extractable uranium (6.09–17.84%), oxidizable uranium (3.33–12.9%) and a higher proportion of residual uranium (70–90%). Overall, the lower-grade ore samples contain a higher proportion of residual uranium, while the higher-grade ore have a higher percentage of weak acid-extractable uranium and pyrite. During mineralization, pyrite could adsorb and reduce the hexavalent uranium of the fluid. If physical and chemical conditions near the ore-bearing rock were changed, the

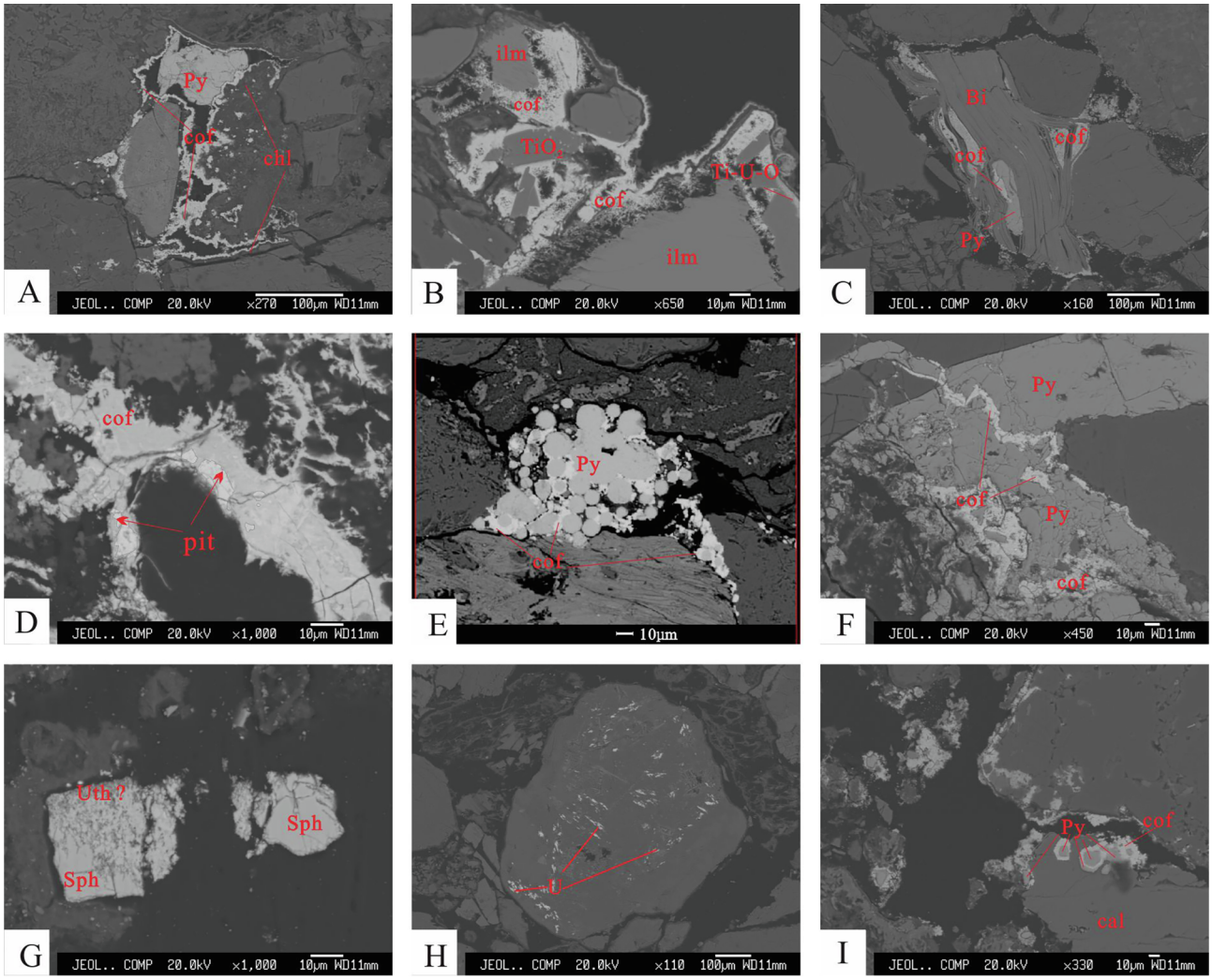

Fig. 4. Main occurrence forms of uranium minerals in uraniferous sandstone of the Tarangaole area. (A) Coffinite grows along clay minerals; it occurs on the periphery of grains. (B) Coffinite are in close association with altered ilmenite, anatase or leucosphenite. (C) Coffinite occur in the cleavage cracks of altered biotite, partly in association with pyrite. (D) The fairly bright pitchblende (?) are wrapped at the core of coffinite. (E) Coffinite grows around strawberry-like pyrite. (F) Veinlet coffinite fill the fissures of pyrite. (G) The lower part of sphene is intact, while the upper fractured part is uraniferous. (H) A certain amount of uranium is present in the rock debris. (I) Granular pyrite is wrapped by a circle of coffinite. And individually, another circle of pyrite is seen on the periphery of coffinite. They are cemented and filled up by calcite. Abbreviations: Py, pyrite; cof, coffinite; pit, pitchblende; Uth, uranothorite; Sph, sphene; ilm, ilmenite; Bi, biotite; chl, chlorite; cal, calcitel; Ti–U–O, uraniferous–titaniferous mineral.

Table 2
Uranium content in the experiment of sequential extraction and their related proportions.

Sample Number	Lithology	Sample Location	Occurrence State of Uranium (ug/g)					Total Uranium Content	Remarks
			G1	G2	G3	G4	G5		
16nzk033	Gray coarse sandstone	UZK(467.1 m)	42.2(4.60%)	317(34.59%)	24.8(2.71%)	84.5 (9.22%)	448(48.88%)	916.5	Present Test
16nzk027	Grayish white coarse sandstone containing carbon dust	UZK(551.3 m)	0.358(0.48%)	10.3(13.75%)	0.281(0.38%)	5.78(7.71%)	58.2(77.68%)	74.9	
16nzk032	Gray coarse sandstone	UZK(466.8 m)	25.1(2.30%)	386(35.41%)	23.9(2.19%)	109(10%)	546(50.09%)	1090	
16nzk043	Gray coarse Sandstone containing carbon dust	UZK(484.5 m)	0.147(0.45%)	5.88(17.84%)	0.074(0.22%)	4.25(12.9%)	22.6(68.59%)	32.95	
16nzk054	Gray carbonaceous coarse sandstone containing boulder clay/carbon dust	UZK(625.8 m)	10.1(1.76%)	191 (33.31%)	6.32(1.10%)	186(32.44%)	183(31.91%)	576.4	
Mean			1.92%	26.98%	1.32%	14.45%	55.43%		
2014DY-15	Light grayish white medium sandstone	ZK105-3	20.2 (4.24%)	81.3(17.06%)	8.06(1.69%)	214(44.91%)	153(32.11%)	476.56	Previous information
HJQ-36	Light gray Medium sandstone	Deng1	1.68(0.39%)	72.5(16.92%)	1.26(0.29%)	210(49.02%)	143(33.38%)	428.40	
2014DY-36	Light gray medium sandstone	ZKC2014-3	30.3(2.86%)	361(34.10%)	33.3(3.15%)	426(40.24%)	208(19.65%)	1058.6	
2014DY-32	Light gray medium sandstone	ZKN51-1	0.332(1.12%)	1.8(6.09%)	0.066(0.22%)	1.18(3.99%)	26.2(88.58%)	29.58	
2014DY-34	Light gray medium sandstone	ZKN24-4	0.105(2.67%)	0.36(9.15%)	0.009(0.23%)	0.131(3.33%)	3.33(84.63%)	3.94	
Mean			2.63%	25.89%	2.14%	42.63%	26.72%		

Note: Analysis for this study was done at the Analytical Laboratory, CNNC Beijing Research Institute of Uranium Geology; previous data are from Wu et al. (2016), and Cun et al. (2016); G1, water-soluble state; G2, weak acid-extractable state; G3, reducible state; G4, oxidable state; G5, residual state.

uranyl complex ion in the fluid would discharge a large amount of uranium, accompanied by the formation of carbonate cement. Thus, this part of uranium would co-exist with the carbonate cement.

5. Discussion

5.1. Chemical composition of main uranium minerals

5.1.1. Two types of coffinite (high-Y and low-Y type)

Some uranium minerals exhibit a high content of Y in their chemical composition. The EPMA data indicates a large variation in the content of Y_2O_3 in coffinite (0–7.3%); this is based on approximately 50 statistical data (Table 1), with most points clustered in a dense region with proportions smaller than 1%, and the rest are distributed between 3.3 and 7 %. Some authors have attributed the presence of coffinite with high-Y content to the involvement of subsequent hydrothermal process (Ma et al., 2013; Wu et al., 2016). However, through an analysis of the front area of the interlayer oxidized zone in Central Asia, it was argued that the element Y migrated in the form of carbonate or sulfuric complexes, and was enriched in the uranium ore zone under the effect of geochemical barriers, such as *pH* and *Eh* (Chen et al., 2010). Although the mechanism of enrichment in this area is not confirmed, the data on chemical composition shows at least two types of coffinite (high-Y and low-Y type) exist in this area. Combined with previous studies on altered minerals and fluid inclusions in this area (Yang et al., 2006a,b), two different fluid-metallogenic events may have affected the region.

5.1.2. Pitchblende

Pitchblende is rarely seen in the area, and usually occurs wrapped around coffinite with irregular serrated boundaries. The average content of UO_2 and SiO_2 in pitchblende was 86.41% and 4.33%, respectively. The reflectivity of pitchblende ranges from 17 to 21 %, while the reflectivity of coffinite is less than 10% (Min et al., 1999). This is the reason why pitchblende appears to be brighter than coffinite. A uranium mineral, most likely ursilite, with UO_2 content of 62.03–71.40% and SiO_2 content of approximately 4.06–9.65% was reported from the Zaohuohao Deposit of the Ordos Basin (Miao et al., 2010). A previous study also revealed that small amounts of uraninite or pitchblende was discovered by X-ray powder diffraction in the uranium ore of the northeast Ordos Basin (Fang et al., 2017). It is most likely residual primary pitchblende, which was probably altered and subsequently, replaced (Min et al., 1992). Furthermore, EPMA data indicate that this mineral and the surrounding coffinite contain little to no Y element. Synthetically, this uranium mineral could be regarded as a residue product, affected by the metallogenic fluid.

5.2. Controls of altered biotite, ilmenite and pyrite on uranium enrichment

5.2.1. Altered biotite

Some lentiform or fine-grained coffinite commonly occur in the cleavage cracks of biotite in uranium ores (Fig. 4C and 6A). In the Dongsheng Deposit, a previous study attributed coffinite to a product that was subsequently reduced and precipitated (Miao et al., 2009, 2010). Our study shows that some coffinite may be associated with pyrite in the cleavage cracks of biotite; their boundaries are very clear (Fig. 4C). During hydrolysis and chloritization, biotite exhibits expansion and loosening, while becoming more adsorbent. A large amount of Fe^{2+} precipitates in this process, creating a micro-reducing environment for uranium reduction and precipitation. U^{6+} and SiO_2 in the fluid are adsorbed, reduced and precipitated subsequently near the cleavage cracks of altered biotite in an alkaline reducing environment. Parts of Fe^{2+} react with S^{2-} or H_2S, producing colloidal pyrite that fills up the cleavage cavities.

5.2.2. Altered ilmenite

The analysis results of heavy minerals indicate that numerous titaniferous minerals exist in the uraniferous sandstone of the Tarangaole area,

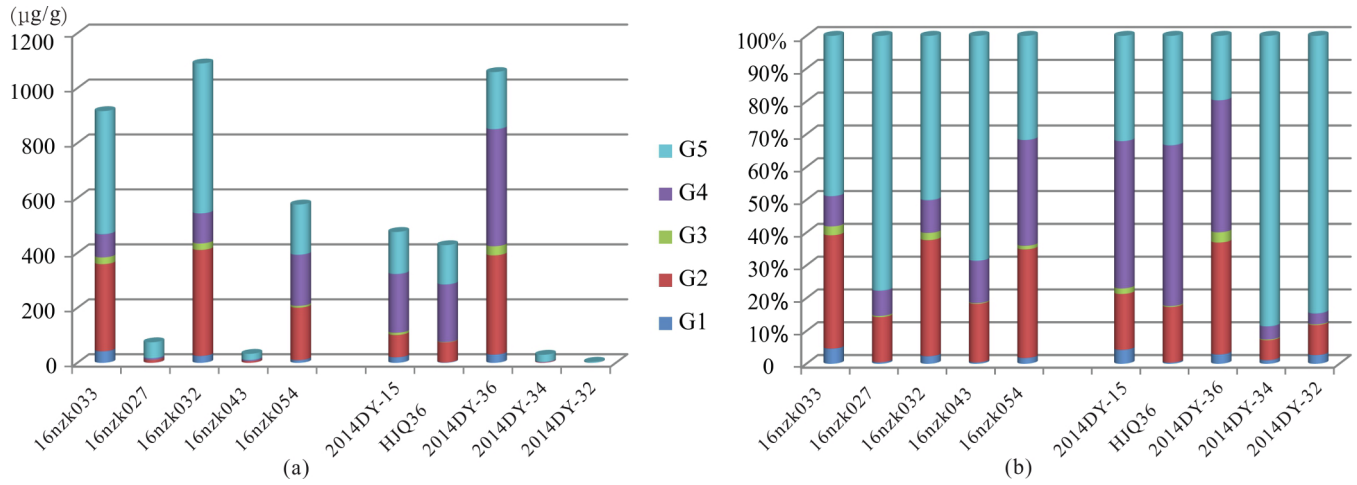

Fig. 5. The ratio of the sequential chemical extraction experiments from uranium ore. (a) Uranium content of various forms in the samples. (b) Relative percentage of various forms of uranium in the samples.

including rutile, ilmenite, anatase and leucosphenite. Backscattering images demonstrate that coffinite grows around rutile, anatase or leucosphenite (TiO_2) as burrs or in micro-columnar form. Most ilmenite display traces of alteration; their mineral textures are disrupted, and their edges are frequently wrapped by coffinite (Fig. 6B and D). While the edges of individual ilmenite appeared relatively intact, there is coffinite and severe alteration visible in the core (Fig. 6C). During mapping analysis using the electron probe, the chemical composition varies remarkably from the core to the edge (Fig. 6E–H). The content of Fe gradually decreases to zero, while the proportion of Ti increases at first and then decreases to zero. Moreover, the content of U gradually increases from zero only at the edge of the mineral. This is a mineral assemblage sequence, with ilmenite, leucosphenite (TiO_2), uraniferous–titaniferous mineral, and coffinite. Furthermore, previous experimental analysis show that some strongly altered ilmenite and intact unaltered ilmenite were also found in non-mineralized sandstone, indicating that the alteration of partial ilmenite began before the metallogenic period.

Previous studies identified a small amount of 'brannerite' in EPMA data of uranium minerals (Wu et al., 2016), which mostly coexisted with altered ilmenite (anatase, TiO_2). It was considered to be a product of ilmenite replaced by coffinite (Wang et al., 2017). This theory originated from the 'Pronto reaction' in the Precambrian quartz conglomerate of the Pongola basin (Min et al., 1992). Uraniferous hydrothermal fluid replaced ilmenite in a thermal environment (220–250 °C), with the reaction occurring inward from the edge of the mineral (Saager et al., 1983; Min et al., 1992). Brannerite is a hypothermal mineral that develops in medium-to-high temperature; it was assumed to be non-existent in the Tarangaole area based on fluid inclusion studies (Yang et al., 2006b; Zhang et al., 2015a,b). There is no reliable evidence on record to support its association with other hydrothermal minerals. Furthermore, considering its relationship with uranium minerals, it was believed that replaced or altered Ti–Fe oxides were the products of various stages of metallogenic and diagenetic alteration (Bonnetti et al., 2015; Jia et al., 2015). They were considered indispensable aggregating agents for uranium metallogenesis in some deposits. The oxidation of ilmenite was a result of the competitive diffusion of Fe and O solid ions (Zhang et al., 2014); during this process Fe ions migrated and diffused outward to grains. Therefore, if the weathering and leaching time was long enough, ilmenite could undergo alteration, and even form anatase (Hebert and Gauthier, 2007; Yang et al., 2016). This is a reasonable explanation for titanium-enrichment and iron-depletion around altered ilmenite (Fig. 6B and D). When altered ilmenite was subjected to the action of hydrocarbon-containing reducing fluids, some pyrite and anatase would form on its periphery; this was considered an important enrichment medium (Reynolds and Goldhaber, 1978; Jia et al., 2015). After reviewing a number of studies on the synthesis of current new materials containing titanium, treatment of nuclear pollution and uranium extraction from sea water (Cui, 1979; Jin et al., 1998; Guo et al., 2016), it was assumed that a certain form of TiO_2 had a very high adsorption capacity for uranium ions. During the process of sedimentation, diagenesis and metallogenesis, altered ilmenite was responsible for geochemically moving out iron, enriching titanium and adsorbing uranium. Part of this adsorbed uranium was adsorbed onto altered leucosphenite (TiO_2), forming minerals like uraniferous leucosphenite (Xu et al., 1983).

5.2.3. Pyrite

Coffinite is closely associated with pyrite, growing around the edge of primary strawberry-like (Fig. 4E) or epigenetic pyrite (Fig. 6I–K). Some individual coffinite is found to fill up pyrite fissures as veins (Fig. 4F). The shape of coffinite and its co-existence with pyrite are clearly visible under SEM (Fig. 6L). Coffinite generally grows around or along the edge of pyrite; its lateral morphology is mostly spiny. The Fe^{2+} in pyrite is believed to play a critical role in the reduction and precipitation of hexavalent uranium (Chen et al., 2007; Liu et al., 2013). The negative valent sulfur (S^{2-}) in pyrite acts as a reducing agent, and together with Fe^{2+}, creates a microzone-reducing environment thereby directly reducing hexavalent uranium.

$$UO_2^{2+} + Fe^{2+} + SiO_2 + 3H_2O \rightarrow USiO_4 + Fe(OH)_3 + 3H^+ \quad (1)$$

$$[UO_2(CO_3)_3]^{4-} + 2Fe^{2+} + SiO_2 + 3H_2O \rightarrow USiO_4 + 2Fe(OH)_3 + 3CO_2 \quad (2)$$

5.3. Implications for uranium enrichment and in-situ leaching

5.3.1. The enrichment mechanism of uranium

Large-scale hypergenic fluid modification, like that seen in the Tarangaole area of the northeast Ordos Basin is beyond the ability of conventional pre-enrichment or adsorption of uranium. EPMA data indicate that coffinite is the major type of uranium mineral in this area. The comparison of α-track etching and backscattering images reveal a close association of uranium minerals with pyrite, altered ilmenite, biotite, organic detritus, calcite and clay minerals (Fig. 7). The intergranular pores of quartz, feldspar and other debris are filled by mostly uranium minerals (Fig. 7a and b). The larger uranium minerals are closely related to pyrite, altered ilmenite and biotite, which are the primary enrichment mediums. Different altered minerals exhibit different enrichment mechanisms for uranium. The Fe^{2+} and S_2^{2-} in pyrite are highly reducible; the altered products of ilmenite and biotite

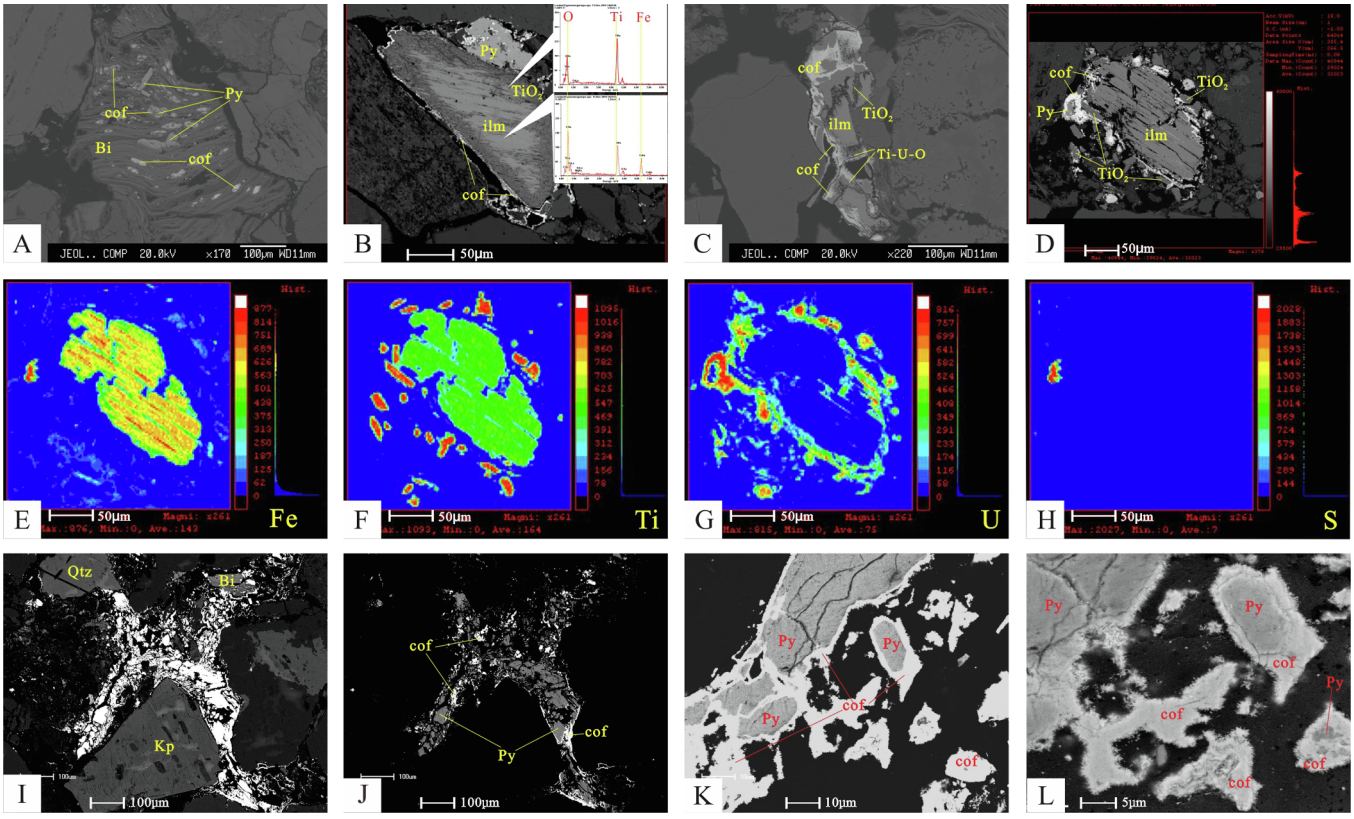

Fig. 6. Uranium occurrence relationship with altered biotite and ilmenite in the Tarangaole area. (A) Coffinite occurs in the cleavage cracks of altered biotite, parts of which coexist with pyrite. (B) The content of Fe in the uraniferous ilmenite reduces from the core to the edge, while the proportion of Ti increases gradually. The content of U increases gradually from zero only at the edge of ilmenite. (C) Coffinite sometimes occurs at the core of altered ilmenite as burrs. (D) Altered core of ilmenite, with uniformly distributed Ti and non-uniformly distributed Fe; it is wrapped by a circle of coffinite that exists in close association with anatase and pyrite on the periphery. (E–F–G–H) Energy spectrometry photographs of Fe, Ti, U, and S. (I–J) Coffinite is closely associated with pyrite along its edge. (K) Coffinite grows along the edge of pyrite, and wraps pyrite. (L) A scanning electron micrograph corresponding to image K; here, the lateral morphology of coffinite is spiny. Abbreviations: Py, pyrite; cof, coffinite; Sph, sphene; ilm, ilmenite; Bi, biotite; chl, chlorite; TiO_2, leucoxene or anatase; Ti–U–O, uraniferous–titaniferous mineral.

not only provide a microreduction environment, but also create the conditions for uranium enrichment and precipitation because of their adsorption capability and storage space. Moreover, the adsorbed uranium is dispersed, and occurs at the edge of grains or in other clay minerals (Fig. 7b and d).

Humic acid and other organic matter are the best mediums to gather uranium because of their complexation behavior and reduction, which forms uranyl ions; they play a critical role in the precipitation and enrichment of uranium (Li et al., 2004; Zhang et al., 2005). Widespread clay minerals in uraniferous sandstone are highly adsorptive to uranium, as seen from the large amounts of star-like uranium in clay minerals over the detrital surface.

Quantitative analysis data indicates that uranium as minerals accounts for a larger proportion as compared to adsorbed uranium, which is largely present in pyrite and organic matter. Furthermore, the lower-grade samples contained a higher proportion of residual uranium, while the higher-grade ore had a higher percentage of weak acid-extractable uranium and pyrite.

Considering these facts, uranium mineralization could be summarized as follows. During the pre-enrichment or early stage of metallogenesis, widespread clay minerals and organic detritus in uraniferous sandstone adsorbed and fixed a large amount of uranium. In the process of supergene epigenetic alteration, with a change in physical and chemical conditions, the uraniferous fluid experienced a complicated successional adsorption–reduction–precipitation process. A major performance was the transformation of hexavalent uranium into tetravalent uranium. First, the uranyl carbonate complex ions of the fluid discharged uranium near the geochemical barrier. This uranium was then absorbed by early pyrite, altered ilmenite, organic matter, biotite and other clay minerals. At the periphery of the above-mentioned minerals, it would have produced a region or microenvironment where the uranium concentration was relatively high. In an alkaline and reducing environment, hexavalent uranium ion and free silicon dioxide were reduced to coffinite. Simultaneously, the redundant ferrous iron reacted with hydrogen sulfide, which made pyrite symbiose with coffinite. Subsequently, carbanions or bicarbonate ions with calcium ions crystallized into carbonate.

5.3.2. *The effect on in-situ leaching*

During the sequential extraction experiment, uranium in G1, G2, G3 and G4 forms were called active uranium, which refers to the leachable portion. Uranium in the residual state (G5) is inertial, and cannot be leached out by conventional methods that use acids or neutral fluids. Lower-grade uranium ores contain a relatively low ratio of active uranium, while not all higher-grade uranium ores contain a high percentage of active uranium (Fig. 5). In situ leaching experiments are being performed in the Nalinggou Zone using the $CO_2 + O_2$ neutral leaching process, where the water-soluble and oxidable state can be leached out. Our findings suggest that if acid addition technology is included in the existing neutral *in-situ* leaching, the result will be much better.

5.4. *Constraints on diagenetic-metallogenic environment and fluid stages*

Unlike a hydrothermal deposit, epigenetic sandstone-type uranium deposits do not display an obvious relationship for interweaved veins or mineral replacements (Fan et al., 2007; Wang et al., 2018). In most cases, the metallogenesis is a long-term accumulative process of

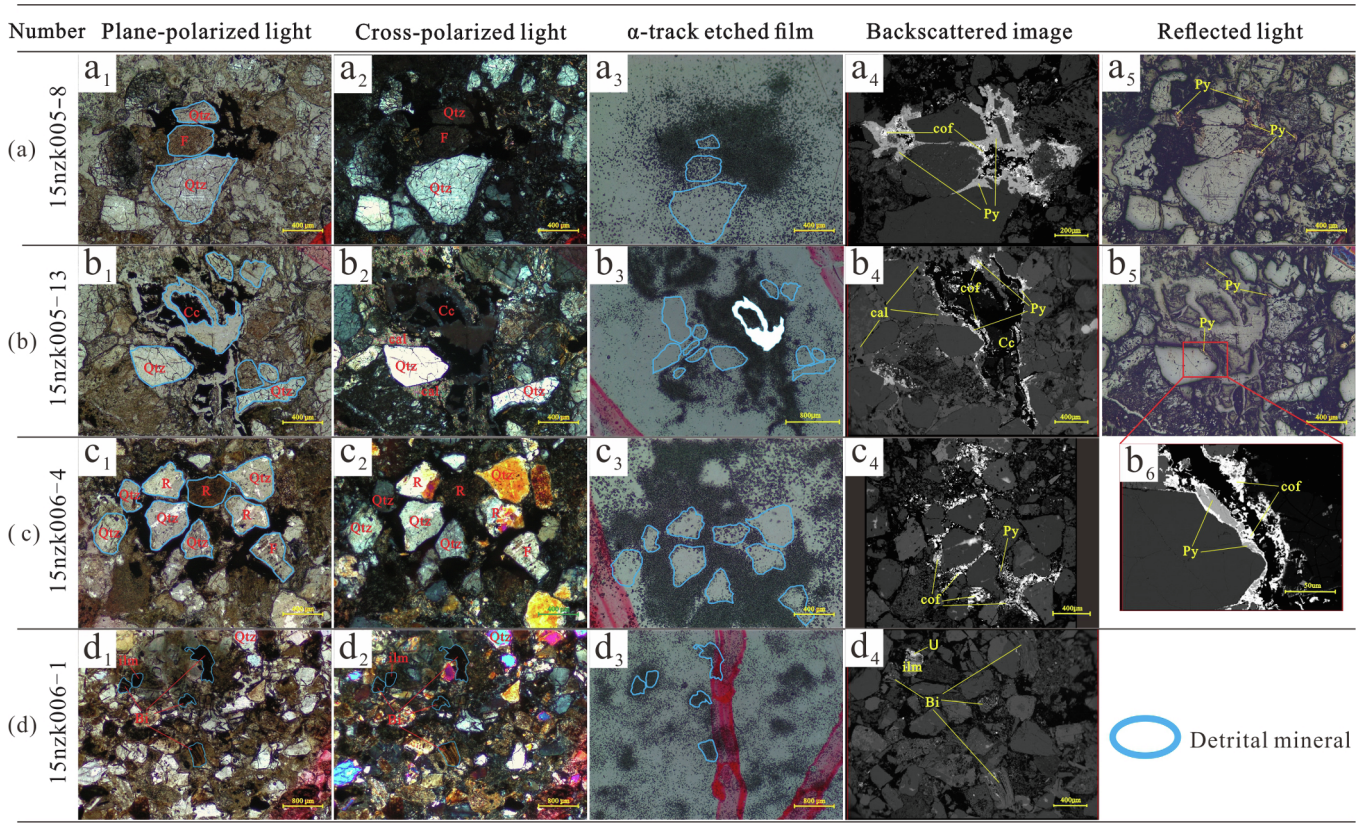

Fig. 7. The relationship between α-tracks and paragenetic minerals from the uranium ore. (a) α-tracks of the film from the thin section 15nzk005-8, with the plane-polarized, cross-polarized, backscattered and reflected light photographs of same scene. In the film, α-tracks are distributed at the edge of pyrite in dense clumps. (b) α-tracks of the film from the thin section 15nzk005-13 are distributed on the periphery of carbonaceous clastics as dense clumps, some of which are associated with pyrite. (c) α-tracks of the film from the thin section 15nzk006-4 are distributed in the intergranular pores in the form of dense clumps. (d) α-tracks of the film from the thin section 15nzk006-1 are mainly distributed on the edge of altered ilmenite and in cleavage cracks of biotite. Other tracks sporadically occur in intergranular pores. Abbreviations: Py, pyrite; cof, coffinite; ilm, ilmenite; Bi, biotite; cal, calcitel; Cc, carbonaceous clastics; R, rock detritus; Qtz, quartz; F, feldspar.

enrichment–migration-re-enrichment, which can last for millions of years or even longer. According to our findings, pitchblende wrapped by coffinite suggests that it developed before coffinite in this area. The fissures of intergranular cemented pyrite were filled with the veined coffinite (Fig. 4F). Two stages of pyrite are shown in Fig. 4I. Most of the granular pyrites were wrapped by a circle of coffinite. Another circle of pyrite was individually seen on the periphery of coffinite. Eventually they were cemented and filled up by calcite. Meanwhile, mass kaolinization in the target layer was also detected in field core samples, and occasionally the subsequent calcite vein was seen to cut through the boulder and pyrite clumps. These findings suggest that the mineral formation sequence was early-stage pyrite and coffinite, followed by late-stage pyrite, and then calcite. The sedimentary diagenetic environment appeared to be partial acidic in the early stage, and partial alkaline in the late stage (Yang et al., 2006a,b; Fan et al., 2007; Chen et al., 2017). Uranium metallogenic events typically occurred in the transition period of fluid environment (Jin et al., 2014).

This area was affected by at least two stages of fluid activity. Evidence for this comes from the characteristic presence of coffinite with high-Y and low-Y, as well as from the existence of coffinite replaced by primary pitchblende. The ore-forming fluids were most likely silicon-poor and silicon-rich, which typically have high-Y and low-Y, respectively. Thus, in this area, multiple stages of fluid activity is an important factor aiding sandstone-type uranium mineralization.

6. Conclusions

(1) In the Tarangaole area, uranium typically occurs either as uranium minerals or in an adsorbed state. The proportion of uranium in mineral form was notably higher than adsorbed uranium; the organic-pyrite bonded state was dominant in adsorbed uranium. The lower-grade samples contained a higher proportion of residual uranium, while the higher-grade ore had a higher percentage of weak acid-extractable uranium and pyrite.

(2) The uranium minerals are typically coffinite, together with some pitchblende and uraniferous–titaniferous minerals. They are closely related to pyrite, organic detritus, altered ilmenite, biotite and clay minerals, which are widely developed in the uraniferous sandstone. Coffinite usually occurs at the edge of mineral grains or in the cleavage of biotite, and as burrs or in micro-columnar form. However, the adsorbed uranium was mainly distributed along the clastic edges, and part of the uranium occurred in organic matter or clay minerals.

(3) The two types of coffinite (high-Y and low-Y), and the symbiotic relationship of altered minerals indicate that the uraniferous sandstone underwent multiple periods of fluid activity in this area. The complex adsorption–reduction–precipitation during multiple stages of fluid activity lead to mineralization and could be the main enrichment mechanism of uranium in the Tarangaole area of the northeast Ordos Basin.

Acknowledgments

This study was financially supported by projects under the National Key Infrastructure Development Plan (2015CB453006), the National Youth Natural Science Foundation (41502195), the National Key Research and Development Program of China (2018YFC0604200), and the project of China Geological Survey (DD20190119, DD20190121).

We thank Director Xu Tiemin and Mr. Zheng Zhikang of the Tianjin Center of the China Geological Survey, Dr. Zhang Xin of the East China Institute of Technology, and Mr. Ge Xiangkun of the CNNC Beijing Research Institute of Uranium Geology for their guidance . We also thank Dr. Franco Pirajno, Dr. Xiaoyong Yang, and the two anonymous reviewers for their constructive comments and suggestions which helped improve the manuscript.

References

Akhtar, S., Yang, X., Pirajno, F., 2017. Sandstone type uranium deposits in the Ordos Basin, Northwest China: a case study and an overview. J. Asian Earth Sci. 146, 367–382.

Bonnetti, C., Cuney, M., Michels, R., Truche, L., Malartre, F., Liu, X., et al., 2015. The multiple roles of sulfate-reducing bacteria and Fe-Ti oxides in the genesis of the Bayinwula roll front-type uranium deposit, Erlian basin. NE China. Econ. Geol. 110 (4), 1059–1081.

Chen, L.L., Feng, X.X., Sima, X.Z., Li, J.G., Guo, H., Chen, Y., Zhao, H.L., Tang, C., Wang, G., Liu, Z.R., Li, S.G., 2017. Occurrence forms of the uranium minerals in the Nalinggou area of the Ordos basin and geological implications. Geol. Explor. 53 (4), 632–642 (in Chinese with English abstract).

Chen, Z.Y., Guo, Q.Y., 2007. Mechanism of U-reduction and concentration by sulphides at sandstone-type uranium deposits. Uranium Geol. 23 (06), 321–327 (in Chinese with English abstract).

Chen, Z.Y., Guo, Q.Y., 2010. The mechanism of rare elements concentration in the redox front area of interlayer oxidation type sandstone-hosted uranium deposits. Uranium Geol. 26 (1), 1–8 (in Chinese with English abstract).

Chen, D.S., Li, S.X., Cai, Y.Q., 2003. A discussion on research situation and development direction of sandstone-type uranium deposits in the Meso-Cenozoic basin of China. Acta Sedimentol. Sin. 1, 113–117 (in Chinese with English abstract).

Cui, Q.C., 1979. The absorption mechanism of uranium in sea water on hydrous titanium oxide. Oceanol. Limnol. Sin. 2, 119–124 (in Chinese with English abstract).

Cun, X.N., Wu, B.L., Zhang, H.S., Sun, L., Luo, J.J., Li, Y.Q., Pang, K., Zhang, Q., 2016. Study on uranium occurrence state of Daying sandstone-type uranium deposits in Ordos Basin. Northwest Geol. 49 (2), 198–212 (in Chinese with English abstract).

Decree, S., Deloule, E., De Putter, T., Dewaele, S., Mees, F., Yans, J., Marignac, C., 2011. SIMS U-Pb dating of uranium mineralization in the Katanga Copperbelt: constraints for the geodynamic context. Ore Geol. Rev. 81–89.

Doveton, J.H., Merriam, D.F., 2004. Borehole petrophysical chemostratigraphy of Pennsylvanian black shales in the Kansas subsurface. Chem. Geol. 206, 249–258.

Fan, A.P., 2007. Mineralization constraints of jurassic diagenesis in dongsheng uranium mining area. Ordos Basin. Northwest Univ. 1–162 (in Chinese with English abstract).

Fang, X.H., Li, Z.Y., 2017. Research on coffinite in Dongsheng uranium field. Uranium Geol. 33 (5), 257–265 (in Chinese with English abstract).

Galindo, C., Mougin, L., Fakhi, S., Nourreddine, A., Lamghari, A., Hannache, H., 2007. Distribution of naturally occurring radio nuclides (U, Th) in Timahdit black shale (Morocco). J. Environ. Radioactivity. 92, 41–54.

Gallegos, T.J., Campbell, K.M., Zielinski, R.A., 2015. Persistent U(IV) and U(VI) following in-situ recovery (ISR) mining of a sandstone uranium deposit, Wyoming. USA. Appl. Geochem. 63, 222–234.

Granger, H.C., Warren, C.G., 1974. Zoning in the altered tongue associated with roll-type uranium deposits. In: Formation of Uranium Ore Deposit. IAEA, pp. 185–200.

Guo, Y.D., Jiang, H.O., Bu, X.Z., Fu, X.T., Gao, B., Ma, W.J., 2016. Low-temperature synthesis and photocatalytic reduction of U(VI) of anatase TiO_2. J. Ceram. 3, 283–288 (in Chinese with English abstract).

Hebert, E., Gauthier, M., 2007. Unconventional rutile deposits in the Quebec Appalachians: product of hypogene enrichment during low-grade metamorphism. Econ. Geol. 102 (2), 319–326.

Jia, H., Liu, K.P., Li, B.X., Yu, H.W., Yin, L.F., Wang, K., 2015. Uranium occurrence and mineral assemblage characteristics of uranium deposit in Huianbu Area. Uranium Geol. 31 (4), 432–437 (in Chinese with English abstract).

Jin, Q.S., Song, Y.J., Song, D.K., Jiang, L.Q., Zhao, A.M., 1998. The sorption of uranium on crystalline TiO_2 and composite modification TiO_2-SiO_2 and the irradiation stability of the studied materials. J. Nucl. Radiochem. 2, 17–21 (in Chinese with English abstract).

Jin, R.S., Zhang, C.J., Feng, X.X., Tao, C., Zhu, Q., Li, G.Y., 2014. The influence of fluid mixing on the mineralization of sandstone type uranium deposits. Geol. Bull. China. 33 (2/3), 354–358 (in Chinese with English abstract).

Li, S.F., Zhang, Y., 2004. Formation mechanism of uranium minerals at sandstone-type uranium deposits. Uranium Geol. (02), 80–84 (in Chinese with English abstract).

Liu, J., Nie, F.J., Hou, S.R., Chen, L.L., Wang, J.L., 2013. Types of uranium mineral and its occurrence state of the sandstone-type uranium deposits in the Meso-cenozoic basin. J. East China Inst. Technol. Nat. Sci. 36 (02), 107–112 (in Chinese with English abstract).

Ma, Q., Feng, Z.G., Sun, J., Xie, E.J., Li, X.J., 2012. Study on chemical speciation of uranium in samples from in-situ leaching sandstone-type uranium deposit in Xinjiang. Rock Miner. Anal. 31 (3), 133–138 (in Chinese with English abstract).

Ma, Y., Wu, B.L., Liu, Y.F., Liu, C.Y., Zhao, Z.P., Wang, H.T., Song, Z.S., Wei, A.J., 2013. Study on uranium occurrence state of sandstone-type uranium in HJQ region. Ordos Basin. Northwest. Geol. 46 (2), 141–152 (in Chinese with English abstract).

Miao, A.S., Lu, Q., Liu, H.F., Xiao, P., 2009. Occurrence and formation of coffinite in ancient interlayer oxidizing zone of sandstone type U-deposit in Ordos Basin. Geol. Sci. Technol. Inf. 28 (4), 51–58 (in Chinese with English abstract).

Miao, A.S., Lu, Q., Liu, H.F., Xiao, P., 2010. Electronic microscopy study on the uranium minerals of Dongsheng sandstone-type uranium deposit in Ordos Basin. Geoscience 24 (4), 785–792 (in Chinese with English abstract).

Min, M.Z., Zhang, F.S., Zhao, F.M., Wang, D.Y., 1992. Genesis of Uranium Mineralogy Studies. Atomic Energy Press, Beijing, pp. 1–343 (in Chinese with English abstract).

Min, M.Z., Wu, Y.W., Zhang, E.L., Zhang, G.H., Geng, J.H., 1999. A densely zoned rhythmically intergrowth of coffinite and pitchblende and its genetic significance. Acta Mine. Sin. 19 (1), 15–19 (in Chinese with English abstract).

Qin, Y., Zhang, W.Z., Peng, P.A., Zhou, Z.J., 2009. Occurrence and concentration of uranium in the hydrocarbon source rocks of Chang 7 member of Yanchang Formation. Ordos basin. Acta Petrol. Sin. 25 (10), 2469–2476 (in Chinese with English abstract).

Reyes-Cortés, M., Fuentes-Cobas, L., Torres-Moye, E., Esparza-Ponce, H., Montero-Cabrera, M.E., 2010. Uranium minerals from the San Marcos District, Chihuahua. Mexico. Miner. Petrol. 99, 121–132.

Reynolds, R.L., Goldhaber, M.B., 1978. Iron-titanium oxide minerals and associated alteration phases in some uranium-bearing sandstones. J. Res. U.S. Geol. Survey 6 (6), 707–714.

Saager, R., Stupp, H.D., 1983. U-Ti phases from Precambrian quartz-pebble conglomerates of the Elliot Lake area, Canada, and the Pongola basin. South Africa. Tscher. Miner. Petrog. 32 (2–3), 83–102.

Song, Z.S., 2013. Geochronology of sandstone type uranium mineralization in Hangjinqi Erdos basin and its geological significance. Northwest Univ. 20–27 (in Chinese with English abstract).

Song, Z.L., Liu, C.Q., Peng, B., Yang, C., 2004. Sequential extraction (SEE) technology and its applications to sediment and soil element speciation studies. Earth Environ. 32 (2), 70–77 (in Chinese with English abstract).

Wang, J.G., Ma, Y.Y., Tang, G.P., Zhang, Y.T., Pang, W.J., Yao, Y.J., Qiu, L.F., Guo, J., 2018. Study on composition feature polymetallic minerals and metallogenic stages of Niutoushan area, Xiangshan uranium field. World Nucl. Geosci. 35 (3), 143–149 (in Chinese with English abstract).

Wang, Z.X., Min, M.Z., 1989. Uranium Mineral Studies. Atomic Energy Press. 15–32 (in Chinese with English abstract).

Wang, G., Wang, Q., Miao, A.S., Jiao, Y.Q., Yi, C., 2017. Characteristic of uranium minerals in Nalinggou uranium deposit or Ordos Basin and their formation mechanism. Acta Miner. Sin. 37 (4), 461–468 (in Chinese with English abstract).

Wu, B.L., Zhang, W.Y., Song, Z.S., Cun, X.N., Sun, L., Luo, J.J., Li, Y.Q., Cheng, X.H., Sun, B., 2016. Geological and geochemical characteristics of uranium minerals in the sandstone-type uranium deposits in the north of Ordos Basin and their genetic significance. Acta Geol. Sin. 90 (12), 3393–3407 (in Chinese with English abstract).

Xu, J.L., Liu, Y.P., 1983. A new uraniferous mineral: Uraniferous leucosphenite. Radioact. Geol. 1, 14–16 (in Chinese with English abstract).

Xu, Z., Wu, R.G., Cai, J.F., Gong, W., Ning, J., Yu, D., 2010. Application of alpha track etching in research of sandstone-type uranium ore: A case of study in sandstone-type uranium deposit of Tongliao area. J. East China Inst. Technol. Nat. Sci. 33 (1), 9–14 (in Chinese with English abstract).

Xue, W., Xue, C.J., Chi, G.X., Peng, Y.B., Wang, K., 2010. Trace element and REE geochemical characteristics of sandstone-type uranium deposit in the Dongsheng area of the Ordos Basin, China. Geoscience 4, 776–784 (in Chinese with English abstract).

Yang, J.J., 2002. The tectonic evolution and hydrocarbon distribution of Ordos Basin. Petroleum Industry Press, Beijing, pp. 1–220 (in Chinese with English abstract).

Yang, J.P., Dong, T.S., Tang, Y.H., Hu, H.X., 2016. Mineral processing research on low-grade Ti-bearing eluvial placer ore. Multipurpose Util. Miner Resour 5, 34–38 (in Chinese with English abstract).

Yang, X.Y., Ling, M.X., Sun, W., Miao, J.Y., Liu, C.Y., 2006b. Characteristics of fluid inclusions in sandstone- type uranium deposit of Ordos basin. Acta Petrol. Sin. 27 (6), 28–33 (in Chinese with English abstract).

Yang, X.Y., Ling, M.X., Sun, W., 2006a. Study on the ore-forming condition and occurrence of uranium minerals in sandstone-type uranium deposits from Ordos basin, Northwest China. Geochim. Cosmochim. Acta. 70 (18), A720 (in Chinese with English abstract).

Yang, X.Y., Ling, M.X., Lai, X.D., Sun, W., Liu, C.X., 2009. Uranium mineral occurrence of sandstone-type uranium deposits in the Dongsheng-Huanglong region. Ordos Basin. Acta Geol. Sin. 83 (8), 1167–1177 (in Chinese with English abstract).

Zhang, J.B., 2014. Phase and microstructure changes of Panzhihua ilmenite during oxidation-reduction pretreatment and their influence mechanisms on the hydrochloric acid leaching. Univ. Chin Acad. Sci. 1–129 (in Chinese with English abstract).

Zhang, L., Liu, C.Y., Zhao, Z.P., Wang, F.F., Song, Z.S., 2015a. Fluid evolution and mineralization of Hangjinqi sandstone-type uranium deposit. Ordos basin. Earth Sci. Front. 22 (3), 368–381 (in Chinese with English abstract).

Zhang, X., Nie, F.J., Zhang, C.Y., Zhang, H.J., Dong, F.S., Lu, Y.Y., 2015b. Study on uranium occurrence state of sandstone-type uranium deposits in Mengqiguer deposit. Yili Basin. Sci. Technol. Eng. 15 (33), 18–24 (in Chinese with English abstract).

Zhang, J.Y., Wang, A.Z., Li, X.Y., Zheng, Z.X., Li, J.Z., 1995. Uranium Mineralogy of China. Atomic Energy Press, Beijing, pp. 3–282 (in Chinese with English abstract).

Zhang, M.Y., Zheng, J.W., Tian, S.F., Xia, Y.L., Liu, H.B., 2005. Research on existing state of uranium and uranium ore-formation age at Qianjiadian uranium deposit in Kailu depression. Uranium Geol. 21 (4), 213–218 (in Chinese with English abstract).

Zhao, K.D., Jiang, S.Y., Chen, W.F., Chen, P.R., Ling, H.F., 2014. Mineralogy, geochemistry and ore genesis of the Dawan uranium deposit in southern Hunan Province, South China. J. Geochem. Explor. 138, 59–71 (in Chinese with English abstract).

Zheng, J., Jia, Z.K., Wang, X.N., Yang, B.F., Song, J., Zeng, X., Feng, Y., Ma, Q., Hu, Y., 2015. Application of sequential extraction method in the analysis of chemical speciation of uranium. Inn. Mongolia Petrochem. Ind. 15, 1–2 (in Chinese with English abstract).